

Superheating of Small Solid-Argon Bubbles in Aluminum

C. J. Rossouw and S. E. Donnelly

*Division of Chemical Physics, Commonwealth Scientific and Industrial Research Organization,
Clayton, Victoria 3168, Australia*

(Received 25 June 1985)

Small solid-Ar bubbles, formed by the implantation of 50-keV Ar⁺ ions into Al, are observed to melt at 730 K, compared with an equilibrium bulk melting temperature of 250 K. A model based on the suppression of Ar thermal vibrations at the Al interface is used to account for the superheating of 480 K. Measurements on the temperature dependence of diffracted electron intensities from these bubbles yield Debye-Waller factors consistent with an effective Debye temperature of about 140 K, compared with a bulk value of 110 K.

PACS numbers: 63.70.+h, 64.70.Dv

Recently, electron diffraction patterns have been used to identify the presence of small solid precipitates or "bubbles" of xenon and argon implanted into aluminum at room temperature.^{1,2} Lattice images of solid Xe bubbles³ reveal undefected as well as defected areas, and the presence of dislocations within Xe bubbles has been confirmed by the matching of optically processed lattice images with dynamical multislice calculations.⁴ In this Letter we report the superheating of Ar bubbles (of mean diameter ~ 2.7 nm) by 480 K, as evidenced by the disappearance of Ar {200} beams at 730 K. A simple model, based on the suppression of thermal vibrations of Ar atoms near the Ar-Al interface, is developed to account for superheating. The attenuation of diffracted intensities with increasing temperature T is used to measure the Debye-Waller factor, which in turn is related to an effective Debye temperature Θ .

The intensity $I_{\mathbf{g}}$ of a diffracted beam \mathbf{g} is attenuated by the Debye-Waller factor⁵ $\exp(-2M_{\mathbf{g}})$, where $M_{\mathbf{g}} = 2\pi^2 g^2 \langle u_{\mathbf{g}}^2 \rangle$ and $\langle u_{\mathbf{g}}^2 \rangle$ is the projection of the mean-square atomic displacements $\langle u^2 \rangle$ along \mathbf{g} . This may be related to the Debye temperature Θ by substitution of a value $\langle u_{\mathbf{g}}^2 \rangle = 3\hbar^2 F(x)/M_a k_B \Theta$ in the Debye-Waller factor, where M_a is the atomic mass, k_B the Boltzmann constant, $x = \Theta/T$, and⁶

$$F(x) = \frac{1}{4} + \frac{1}{x^2} \int_0^x \frac{\zeta d\zeta}{\exp(\zeta) - 1}. \quad (1)$$

In the high- T limit, $F(x) \rightarrow T/\Theta^2$.

A 50-nm-thick, (100) epitaxial Al film was prepared by vacuum evaporation onto a hot (490 K) NaCl substrate. 50-keV Ar⁺ ions were implanted at room temperature into these films to a fluence of 10^{20} ions m⁻², prior to removal from the NaCl and collection onto 400-mesh grids. A 200-keV electron beam was used for lattice imaging and for the recording of diffraction patterns. The intensity of relatively weak Ar beams ($\sim 2\%$ of the Al beam intensities) was measured as a function of temperature in the range $88 \text{ K} < T < 423 \text{ K}$ by use of a Gatan double-tilt heating-cooling holder

in the JEOL 2000 EX electron microscope. Specimens were transferred to a JEOL heating holder for higher-temperature measurements. The incident beam intensity was recorded on the viewing screen before a series of diffraction patterns were taken. Care was taken to calibrate the response of the photographic film to beam intensity, and exposure times were chosen such that densitometry was performed in the linear-response region for the density-versus-dose calibration curve.

For near-symmetrical [001]-zone-axis orientations, dynamical coupling increased the neighboring Al 200 and 220 beam intensities, which in turn increased diffuse background as well as reducing the intensities of Ar diffracted beams. In these circumstances, dynamical diffraction phenomena lead to departures from the kinematical attenuation of diffracted beams,⁷ introducing a possible error of $\sim 10\%$ in attenuation over the temperature range 100–600 K. The specimen was tilted by 6° from the [001] zone axis: This reduced dynamical errors in attenuation compared with the kinematical expression to $\sim 2\%$, and increased the peak-to-background ratio for diffracted Ar beams.

About 10^7 Ar bubbles were within an area of $11 \mu\text{m}$ diameter (the area enclosed by the selected-area aperture), and these lead to the formation of relatively weak diffracted beams. These indicated the presence of epitaxial fcc argon precipitates with lattice parameter $a_0 = 0.516 \pm 0.005 \text{ nm}$ (molar volume $V_m = 20.7 \pm 0.6 \text{ cm}^3$). The Ar {200} beams were no longer detectable at $730 \pm 20 \text{ K}$: We use this criterion to define the melting temperature T_m of the bubbles. If the vanishing of {111} beams near a different zone axis were used to define T_m , this value would be somewhat larger. Within the uncertainty limits for V_m , the equilibrium bulk melting temperature for Ar is⁸ $T_{mb} = 250 \pm 40 \text{ K}$. The bubbles may thus be superheated by about 480 K, i.e., $T_m/T_{mb} \sim 2.8$.

A densitometer trace across 200 and 220 Ar beams for three temperatures is shown in Fig. 1. An analysis of fifty lattice-imaged bubbles yielded a mean diameter

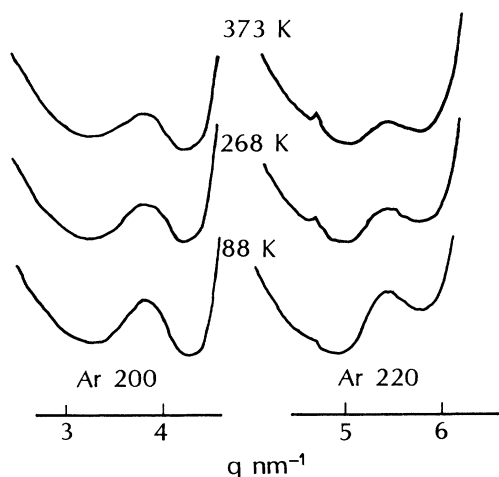


FIG. 1. Densitometer traces of Ar 200 and 220 beam intensities for various temperatures T , scanning radially outwards from $q = 0$.

$D = 2.7$ nm, with a standard deviation of about 0.5 nm. We would expect the half-width $q_{1/2}$ of the diffracted beam, measured radially outwards from 000, to be dependent on g if a variation in lattice parameter, as reported by vom Velde *et al.*,² were to provide a significant contribution. However, a T -independent half-width $q_{1/2} \sim 0.5$ nm⁻¹ for both reflections was observed, consistent with the bubble-shape transform.

Figure 2 shows a plot of I_g vs T , where the beam intensities are scaled to unity at $T = 0$ K. On the har-

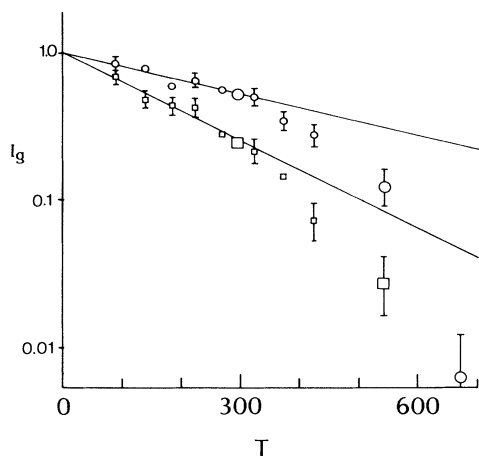


FIG. 2. Plot of I_g vs T for 200 (circles) and 220 (squares) beams. I_g is plotted on a logarithmic scale, with the assumption of a value of unity for the extrapolated $T = 0$ K intensity for each beam. Fitted values from the high-temperature stage are indicated with larger symbols. Solid lines are derived from a least-mean-squares fit to the data below 320 K.

monic approximation⁹ $\langle u^2 \rangle \propto T$, and a least-mean-squares analysis of the 200-beam data in the range 88–320 K, based on a linear relationship between $\ln I_g$ and T , was consistent with $\Theta = 144$ K. A similar analysis of the 220-beam data yielded $\Theta = 139$ K. This compares with $\Theta_b \sim 70$ K for Ar near its bulk melting point $T_{mb} = 83$ K at atmospheric pressure, and $\Theta_b \sim 110$ K for Ar with the same molar volume as measured in the bubbles.¹⁰ It has been shown that the relationship $M_g \propto T^{3/2}$ accounts for anharmonic effects over an extensive temperature range in many crystals,¹¹ although anharmonicity may also be accounted for by a T -dependent Debye temperature. Above 320 K, deviations from linearity in Fig. 2 indicate a breakdown of the harmonic approximation: This effect may be enhanced since a large proportion of argon atoms are in the Ar-Al interface and experience an asymmetric potential well. A plot of $\langle u_g^2 \rangle$ vs T is shown in Fig. 3, with the solid line derived from $\Theta = 141.5$ K for Ar. Note that the measured rms displacements fall between values for Al¹² and bulk Ar at atmospheric pressure.

In order to account for the thermal behavior of the argon bubbles, we follow arguments analogous to those of Pietronero and Tosatti¹³ in which thermal

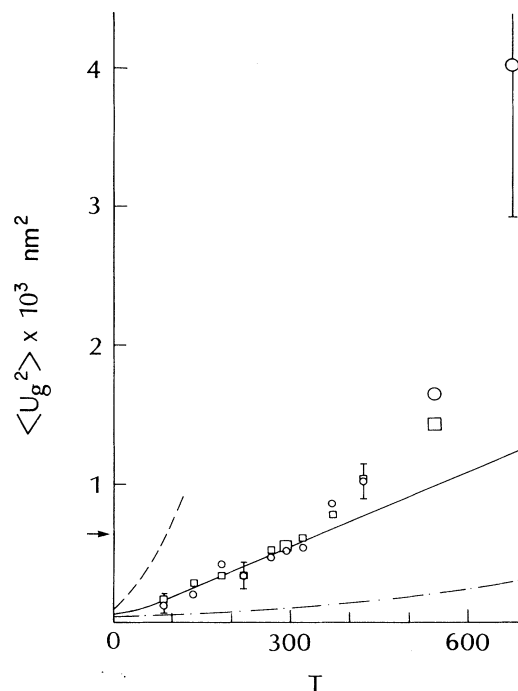


FIG. 3. Plot of $\langle u_g^2 \rangle$ vs T , as derived from 200 (circles) and 220 (squares) Ar beams. Data for Al (dash-dotted line) and solid Ar at atmospheric pressure (dashed line) are indicated, as well as a fit by $\Theta = 141.5$ K (solid line) for Ar. The value set by the Lindemann criterion for the mean-square displacement of bulk Ar at melting is indicated by the arrow.

characteristics of atoms vary with distance from a surface. Assigning different mean-square displacements $\langle u_j^2 \rangle$ along \mathbf{g} for various atomic layers j , we coherently sum the contribution to the diffracted beam amplitude from atoms in each layer j . This leads to a relationship

$$\begin{aligned} & \exp(-2\pi^2 g^2 \langle u_g^2 \rangle) \\ &= \sum_j r_j \exp(-2\pi^2 g^2 \langle u_j^2 \rangle), \end{aligned} \quad (2)$$

where r_j is the proportion of atoms in the j th layer and, unlike the approach adopted by Harada and Ohshima,¹⁴ the exponential terms are not expanded to first order. From lattice-image information, a regular octahedron bounded by $\{111\}$ planes is representative of the shape of a typical solid inert-gas bubble.³ Assuming seven atoms along outer $\langle 110 \rangle$ directions in the $[001]$ projection (linear dimension 2.55 nm), the proportion of surface atoms is $r_s = 0.632$. For $T \sim 200$ K, with an abrupt change to bulk behavior for argon atoms not in the aluminum interface, we have $\Theta_s \sim 177$ K if $\Theta = 141.5$ K and $\Theta_b = 110$ K. This compares with a Debye temperature of 398 K at 200 K for aluminum.¹¹

Superheating is accounted for by adopting an approach similar to the one used by Hoshino and Shimamura¹⁵ for the size dependence of T_m for fine particles. Firstly, the average mean-square displacement is written as a sum of contributions from different layers j , i.e.,

$$\langle u_g^2 \rangle = \sum_j r_j \langle u_j^2 \rangle. \quad (3)$$

Secondly, melting is assumed to take place when $\langle u_g^2 \rangle$ exceeds a critical value. For the high-temperature limit of the Debye model, Eq. (3) may be rewritten in terms of a bulk melting temperature T_{mb} ($r_b \rightarrow 1$) compared to the bubble T_m for an equivalent average mean-square displacement. This yields

$$T_{mb}/\Theta_b^2 = T_m \sum_j r_j / \Theta_j^2. \quad (4)$$

Thus superheating is predicted for $\Theta_j > \Theta_b$, as opposed to a reduction in T_m when $\Theta_j < \Theta_b$ as in the case of small free particles.¹⁵ With our estimate on the two-layer model of $\Theta_s \sim 1.6\Theta_b$, a suppression in the amplitude of thermal vibrations of Ar atoms in contact with the Al matrix takes place. Equation (4) then yields $T_m/T_{mb} = 1.6$ for r_s and Θ_b as previously estimated. An upper bound on the ratio T_m/T_{mb} for this model is 2.7 as $\Theta_s \rightarrow \infty$. This ratio may be increased if more layers are assumed in the surface-to-bulk transition.

The observed superheating of ~ 480 K is not readily explicable in terms of standard theories of melting. For instance, the Lindemann theory⁹ yields a ratio $\langle u^2 \rangle^{1/2}/R \sim 0.12$ at the melting point of argon (this is indicated in Fig. 3), where $R \sim 0.365$ nm is the nearest-neighbor distance. From Fig. 3, and by use of

the approximate relationship $\langle u^2 \rangle = 3 \langle u_g^2 \rangle$, the largest experimental value for $\langle u^2 \rangle^{1/2}/R$ at 675 K is 0.3 ± 0.1 , an increase of about $2\frac{1}{2}$ when compared with the bulk value at melting.

Couchman and Jesser¹⁶ have given a brief overview of the melting phenomenon, discussed in terms of either the generation of vacancies and interstitials, the spontaneous generation of dislocations, or the absolute mechanical stability of the crystal lattice. As a precursor to melting, defects producing lattice disorder are preferentially nucleated at surfaces or existing defects (e.g., grain boundaries) where the formation energy is lower than that for a perfect crystal.

It has been shown that mean-square displacements of surface atoms normal to the external surface are about 1.8 times the bulk value.¹⁷ This explains why crystals do not reach their theoretical bulk melting temperature T_{mb} , since the vibrational amplitude of an atom on a free surface will exceed a critical (melting) amplitude before those in the bulk.¹⁸ Experimental evidence has recently been obtained for the melting of lead in stages from the surface,¹⁹ starting with some surface disorder a full 100 K below T_{mb} . On the other hand, with the exception of systems with sluggish melting kinetics such as quartz,²⁰ superheating of crystals with uniform composition by more than about 2 K has not been observed. However, superheating of more than 100 K has been observed for small Bi spheres, coated with a surface Sb layer.²¹ A general theory for the melting of such systems (spheres of low T_{mb} coated with a surface layer of high T_{mb}) has been developed²²: Superheating occurs since nucleation of a liquid phase is constrained to take place within the bulk rather than at a free surface. Some similarities exist between this system and the Ar bubbles in aluminum (i.e., a small crystal coated with a higher- T_m material). NMR studies²³ have also revealed considerable superheating in bubbles (~ 2 nm diameter) of molecular hydrogen in a α -silicon matrix.

Evans and Mazey²⁴ have monitored the diffracted electron beam intensity from solid Kr bubbles (diameter ~ 3 nm) in Cu and Ni as a function of temperature: The intensity disappeared at 850 K in Ni ($V_m = 18.8$ cm³) and 575 K in Cu ($V_m = 21.2$ cm³). According to our calculations, based on the work of Anderson and Swenson,²⁵ these figures represent a depression in the melting temperature of Kr, compared with the bulk values, of about 200 and 100 K, respectively. An increase in the lattice parameter of the Kr bubbles was observed by Evans and Mazey after cycling through the melting point, indicating the diffusion of vacancies from the host metal matrix to the bubbles. The likelihood of superheating would be reduced by the availability of free volume at the metal-bubble interface. We observed no increase in the Ar-bubble lattice parameter on cycling through the

melting point.

In conclusion, we have experimental evidence that thermal vibrational amplitudes of argon, present in small bubbles in aluminum, are suppressed when compared with bulk values for argon with a similar molar volume. Electron beams continue to be diffracted from these bubbles at temperatures well in excess of the bulk melting temperature, indicating a superheating of about 480 K. A simple model based on a change from surface to bulk thermal characteristics within the bubbles is able to predict superheating, although the rms displacements near T_m exceed those predicted on the Lindemann criterion by a factor of $2\frac{1}{2}$. A prediction of the thermal behavior of the small Ar bubbles from macroscopic thermodynamic properties may not be valid, given that (60–70)% of the ~230 atoms in each bubble are in the Ar-Al interface.

We thank T. Bastow, R. Elliman, S. Mair, A. McL. Mathieson, A. Moodie, and S. Wilkins for suggestions and fruitful discussions. We are indebted to P. Hanan and A. Spargo of the Department of Physics, University of Melbourne, for the loan of the cold stage.

¹C. Templier, C. Jaouen, J-P. Rivière, J. Delafond, and J. Grillé, *C. R. Acad. Sci.* **299**, 613 (1984).

²A. vom Velde, J. Fink, Th. Muller-Heinzerling, J. Pfluger, B. Scheerer, G. Linker, and D. Kaletta, *Phys. Rev. Lett.* **53**, 922 (1984).

³S. E. Donnelly and C. J. Rossouw, *Science* (to be published).

⁴S. E. Donnelly, C. J. Rossouw, and I. J. Wilson, *Radiat. Eff.* (to be published).

⁵E. E. Castellano and P. Main, *Acta Crystallogr. Sect. A* **41**, 156 (1985).

⁶D. S. Gemmel, *Rev. Mod. Phys.* **46**, 129 (1974).

⁷C. J. Rossouw and S. E. Donnelly, to be published.

⁸R. K. Crawford, in *Rare Gas Solids*, edited by M. L. Klein and J. A. Venables (Academic, London, 1977), Vol. II, p. 685.

⁹B. T. M. Willis and A. W. Pryor, *Thermal Vibrations in Crystallography* (Cambridge Univ. Press, London, 1975), pp. 142–174.

¹⁰P. Korpiun and E. Luscher, *Rare Gas Solids*, edited by M. L. Klein and J. A. Venables (Academic, London, 1977), Vol. II, p. 711.

¹¹T. J. Bastow, S. L. Mair, and S. W. Wilkins, *J. Appl. Phys.* **48**, 494 (1977).

¹²D. L. McDonald, *Acta Crystallogr.* **23**, 185 (1967).

¹³L. Pietronero and E. Tosatti, *Solid State Commun.* **32**, 255 (1979).

¹⁴J. Harada and K. Ohshima, *Surf. Sci.* **106**, 51 (1981).

¹⁵K. Hoshino and S. Shimamura, *Philos. Mag. A* **40**, 137 (1979).

¹⁶P. R. Couchman and W. A. Jesser, *Philos. Mag.* **35**, 787 (1977).

¹⁷R. E. Allen and F. M. de Wette, *Phys. Rev.* **188**, 1320 (1969).

¹⁸B. Chatterjee, *Nature (London)* **275**, 203 (1978).

¹⁹J. Frenken and J. F. van der Veen, *Phys. Rev. Lett.* **54**, 134 (1985).

²⁰N. G. Ainslie, J. D. Mackenzie, and D. Turnbull, *J. Phys. Chem.* **65**, 1718 (1961).

²¹H. Gleiter, J. H. Perepezko, and K. Smidoda (to be published).

²²A. Holz and H. Gleiter, *Phys. Rev. B* **27**, 1745 (1983).

²³J. B. Boyce and M. Stutzmann, *Phys. Rev. Lett.* **54**, 562 (1985).

²⁴J. H. Evans and D. J. Mazey, *J. Phys. F* **15**, L1 (1985).

²⁵M. S. Anderson and C. A. Swenson, *J. Phys. Chem. Solids* **36**, 145 (1975).